applied sciences

MDPI

Article

Floor Heave Control in Gob-Side Entry Retaining by Pillarless Coal Mining with Anti-Shear Pile Technology

Ivan Sakhno [1,*], Svitlana Sakhno [1], Krzysztof Skrzypkowski [2,*], Oleksandr Isaienkov [1], Krzysztof Zagórski [2] and Anna Zagórska [3]

[1] Faculty of Mining, Donetsk National Technical University, Sofia Kovalevska Street 29, 43012 Lutsk, Ukraine; svitlana.sakhno@donntu.edu.ua (S.S.); oleksandr.isaienkov@donntu.edu.ua (O.I.)
[2] Faculty of Civil Engineering and Resource Management, AGH University of Krakow, Mickiewicza 30 Av., 30-059 Krakow, Poland; zagkrzys@agh.edu.pl
[3] Research Centre in Kraków, Institute of Geological Sciences, Polish Academy of Science, Senacka 1, 31-002 Kraków, Poland; a.zagorska@ingpan.krakow.pl
* Correspondence: ivan.sakhno@donntu.edu.ua (I.S.); skrzypko@agh.edu.pl (K.S.)

Abstract: The severe floor heave in gob-side entry retaining is the major restriction factor of the wide application of pillarless mining thin coal seams. Reinforcement and stress-relief floor heave control methods are the most promising. However, in practice, floor restoration is widely used. Therefore, floor heave control technology in gob-side entry retaining needs to be improved. This study proposes anti-shear pile technology to control floor heave in gob-side entry retaining. The research was mainly carried out by numerical simulation. It was found that the transformation of high vertical stresses in the entry floor underneath the filling wall and coal seam body into horizontal stresses starts the floor heave process. The vertical dilatancy of rocks under the roadway span and their subsequent unloading lead to the delamination of the floor strata and uplift of the entry contour. In this paper, the best pile installation scheme was found. It is a 2pile 5+2 scheme with the installation of two piles, each 2 m long. After that, it was shown that filling piles are more than 3.3 times cheaper than comparable analogs, and pile installation is less labor-intensive. The implementation of the proposed floor heave control method leads to a reduction in heaving by 2.47 times.

Keywords: gob-side entry retaining; pillarless mining; floor heave control; mine roadway stability; thin coal seam mining; steel pile; filling pile; anti-shear pile technology

Citation: Sakhno, I.; Sakhno, S.; Skrzypkowski, K.; Isaienkov, O.; Zagórski, K.; Zagórska, A. Floor Heave Control in Gob-Side Entry Retaining by Pillarless Coal Mining with Anti-Shear Pile Technology. *Appl. Sci.* **2024**, *14*, 4992. https://doi.org/10.3390/app14124992

Academic Editors: Andrea Carpinteri and Paulo Santos

Received: 5 April 2024
Revised: 24 May 2024
Accepted: 5 June 2024
Published: 7 June 2024

1. Introduction

Nowadays, coal provides about a quarter of the world's energy generation. The transition to renewable energy sources is inevitable. However, in reality, the pace of this transition turned out to be slower than expected. The European energy crisis that was caused by the war in Ukraine has shown that in the near future, abandoning coal as an important source of energy is not possible. At the same time, certain types of coal are important raw materials for the metallurgical and chemical industries. Therefore, coal mining will be quite relevant in the near future.

To reduce the negative impact of mining on the environment, governments of various coal-mining countries are introducing increasingly stringent restrictions and environmental regulations. Also, every year, safety requirements in mining become more and more stringent. This leads to an increase in the cost of coal, which stimulates the search and implementation of new technological solutions.

A major part of the world's underground coal is mined from longwall. The US, China, Australia, Poland, and Ukraine use the longwall method. The modern trend in longwall mining is the pillarless mining technology. Its advantages are the following:

- Reduced expenses to mine roadway excavation and, therefore, reduced coal cost;
- An increase in the pace of longwall panel preparation;
- Improvement of the coal recovery ratio;
- Application of effective Y-shaped ventilation systems in the panel, which allows longwall production to be increased by the ventilation factor.

The pillarless method has been known for over 70 years. Experience in its application has been gained in traditional coal-mining countries. Scholars from Germany and Great Britain have made a great scientific contribution to the development of this method [1,2]. Most progress was achieved through the implementation of goaf filling technology and the installation of filling walls. In the 1950s–1960s in Germany, quick-setting materials based on phosphogypsum were developed, from which filling walls were constructed. However, pillarless systems were initially applied with an advancing-type layout of longwall in which gateroads were formed as the coal face advanced (Figure 1a). The majority of such methods were used in thin coal seam mining. However, the absence of a pre-prepared panel and the complexity due to simultaneous roadway excavation and longwall mining in the same panel result in a reduction in the pace of coal mining. Therefore, small coal pillar methods have become more widely used (Figure 1b). In the 1970–1980s, traditional wide pillars were reduced from 20 m to 2–3 m and were applied in many coal basins of Europe and China [3,4]. In the 1970s, Ukrainian mines completely abandoned wide pillars. The elaboration of technologies for the creation of new quick-setting materials has ensured a gradual increase in non-pillar method application (Figure 1c) [5]. Many scholars have researched the efficiency of the filling wall body of gob-side entry retaining in fully mechanized longwalls [6–8].

Additional possibilities for using pillarless methods have appeared in recent years thanks to Chinese scientists. Song and He [9] proposed new pillarless coal-mining technologies. Among them, the N110 construction method is currently the most used pillarless coal-mining technology, which has many advantages [2,10,11]. The essence of this technique is to cut off the connection between the partial roof of the gob and the roof of the roadway by directional roof cutting so that the roof in a certain range above the roadway forms a short-arm beam structure [12].

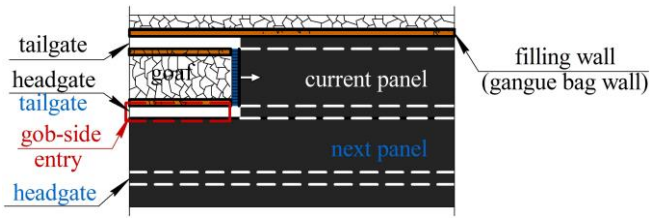

(**a**)

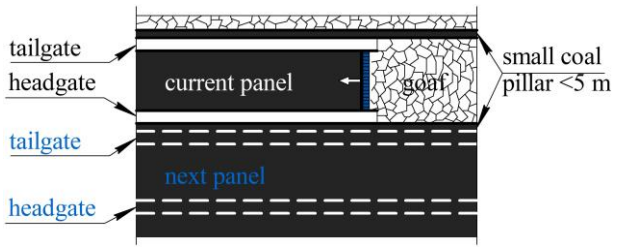

(**b**)

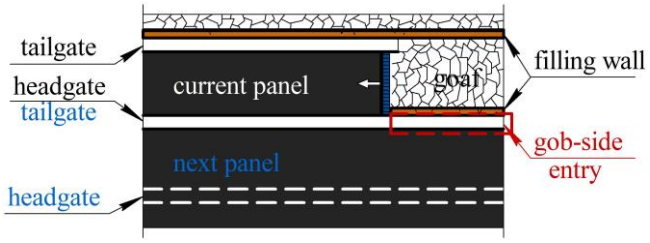

(**c**)

Figure 1. Evolution of thin coal seam longwall mining methods: (**a**)—pillarless method with advancing mining type; (**b**)—small coal pillar method; (**c**)—modern pillarless method.

The widespread application of pillarless coal mining is restricted mainly by the difficulty of ensuring the stability of gob-side entry [13,14]. The problem of gob-side entry retaining stability is aggravated by the constant increase in the mining depth and the natural deterioration of geological conditions. The deformation and failure of the roof and wall sides of the entry in most cases are effectively controlled by a multi-level support system (steel arch, rock bolt, cable bolt), while the entry floor often remains free. Therefore, severe floor heave is an unsolved problem in gob-side entry retaining. Floor heave control will significantly increase the application of progressive pillarless mining technologies.

Many scholars have studied the floor heave mechanism in gob-side entry retaining [15–17]. It can be concluded that failure or plastic flow of the immediate floor, caused by stresses exceeding the strength limit of the rock, is a prerequisite for floor heave [18]. Li et al. [19] pointed out that the key factors of floor heave are changes in the stress–strain state of surrounding rocks after roof failure. This causes an increase in vertical stress in the roadway side walls, which affects the floor strata state. Li et al. 2023 [16] found that the floor is squeezed by the two sides to form an asymmetric sliding force towards the free face of the floor.

Most scientists agree that high horizontal stresses in the immediate floor are one of the main factors that cause severe floor heave. The magnitude of heaving depends on the vertical–horizontal stress ratio [20,21]. Mo et al. [22] proposed the Horizontal Stress Rating (HSR), which represents the magnitude of horizontal stress by statistical analysis on an Australian database. Zhang and Shimada [23] found that variations in the horizontal–vertical stress ratio in the floor strata are the main cause of large floor heave. Gong et al. [15] found that horizontal stress in the immediate floor is the root factor that causes floor heave. Chen et al. [24] proved that squeezing and fluid floor heave play an important role in the stable stage of gob-side entry retaining. Gao et al. [25] defined the main role of shear failure in roadway failure.

Traditional ideas about floor heave identify three main floor heave mechanisms: bearing capacity failure, swelling, and buckling [26]. Each of these mechanisms is associated with a key factor that causes it. Bearing capacity failure cases are associated with the shear failures of the floor strata underneath the coal pillars when the vertical stress exceeds the bearing capacity of the floor. Swelling occurs in wet rocks containing clay minerals. Buckling occurs under the influence of high horizontal stresses on the floor strata [27].

However, in situ, the mechanisms of heaving are not so clear. In gob-side entry retaining, different factors often have simultaneous influence. In each local case, this leads to different magnitudes of floor heave. In addition, the headgate has different media from the two wall sides (solid coal on one side and filling wall on another); it also has different vertical pressure, which leads to asymmetry in the entry deformation.

In this paper, it was accepted that the main cause of floor heave is a change in the stress field in surrounding rocks; moisture is still considered an additional negative factor.

Reinforcement and stress-relief methods have the greatest potential for the control of floor heave in gob-side entry retaining. However, despite the significant scientific substantiation of these methods, in practice, they are not widely used. Floor restoration has been widely implemented. Therefore, scientists from different countries have searched for new effective reinforcement schemes.

Traditional floor reinforcement schemes with rock bolts are modified by combining them with flexible anchor supports [28], shotcrete and steel frames [29], concrete inverted arches [30], pressure-relief holes [31], etc.

Zhu et al. [32] proposed the control method of "bottom lifting + bottom angle bolt + floor bolt" based on the results of a numerical simulation. Wang et al. [33] proposed an asymmetric floor heave control scheme of "floor leveling + anchor cable support + concrete hardening" on the basis of the control principle of "roof + two sides + floor". Wei et al. [34] used 3DEC discrete-element software to simulate and analyze the characteristics and evolution of asymmetric roadway floor heave under dynamic-load disturbance, and proposed the asymmetric control scheme of "slurry anchor reinforcement + top cutting and pressure relief". Zhang et al. [35] used UDEC software to study the floor failure mechanism under the influence of superimposed dynamic and static loads. Full-section anchor cables and inverted arches were proposed to maintain the stability of the surrounding rock. Qin et al. [36] proposed the zonal reinforcement scheme of "fix cable to shed, floor pressure relief, deep-shallow composite grouting" and implemented it in practice, with good results.

It was also proposed to control heaving by installing bolts in the roadway corners. Kang et al. [37] proposed the combined support method of grouting on the floor plate and installing anchor rock bolts in floor corners. Yang et al. [38] studied the mechanical properties of different types of floor corner bolts. However, in high-horizontal-stress conditions, the rock bolts are easy to bend and yield, which reduces the supporting effect.

To control floor heave in gob-side entry retaining, Xu et al. [13] proposed a new steel pile method that was similar to the anti-sliding pile method applied in slope engineering. In this method, steel piles are installed in roadway floor corners before the dynamic pressure zone has an influence.

Kang et al. [39] have shown that the floor angle pile with floor grouting can effectively control the deformation of the roadway floor and two sides. Compared with the rock bolt, the floor corner pile can effectively cut off the sliding line of the floor due to its high bending shear capacity [39]. Guo et al. [40], based on the results of a numerical simulation, field tests, and microseismic monitoring, proposed a floor pressure relief borehole with a large diameter and a concrete-filled steel tube pile support to control floor rock burst. Summing up, it can be seen that floor reinforcement methods in gob-side entry retaining still need to be improved.

This paper is focused on the evolution of floor heave in gob-side entry retaining. Floor heave control with an anti-shear pile method was studied. The numerical simulation with ANSYS code was used for the stress–strain analysis of the surrounding rock. Previous articles researching the effectiveness of pile methods as a method for floor heave control in underground roadways have mainly focused on floor corner piles. The main novelty of this paper is the study of a highly effective floor heave control scheme in which piles were installed not only in the floor corners but in five different positions along the entry span. At the same time, the length and type of the piles varied. Based on the analysis of floor heave causes, promising schemes of pile installation in the immediate floor were proposed and a study of their effectiveness was carried out. As a result, the most effective floor control scheme was determined.

2. Engineering Background

2.1. Geological and Engineering Conditions

The Pivdennodonbasskaya mine is a typical underground coal mine with a depth of 800 m, in the Donbas region of Ukraine. The coal seam has a thickness of 1.3 m and an average inclination of 6°. The immediate roof strata and floor strata of the coal seam are both soft mudstone with thicknesses of 8.2 m and 6.0 m, respectively, as shown in Figure 2a.

Typically, longwall panels have a U-shaped layout where fresh air flows through the headgate to the longwall face, taking away methane, coal dust, and heat, and then flows through the tailgate. At the same time, the small coal pillar method is used with a pillar width of 1.5–3 m. With this system, the daily extraction of coal from the longwall is limited by the gas factor.

Eleven- and twelve-longwall panels have more advanced Y-type longwall mining systems (Figure 2b) based on a retained gob-side entry. Y-type systems contribute to reducing gas accumulation and loss of coal resources in pillars. In Y-shaped systems, fresh air can flow in through two gateroads before the coal face and then flow out through gob-side entry retaining. After the longwall panel mining finishes, gob-side entry retaining can be reused for the next longwall panel.

Column	Lithology	Thickness (m)	Average thinkness (m)	Geologic description, uniaxial strength of intact rock σ_c, (MPa)
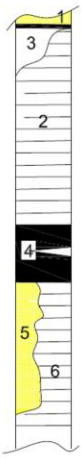	1. sandstone	6.7–8.1	7.4	gray, horizontal bedding, σ_c=57 MPa
	2. sandy mudstone	6.2–10.4	8.2	gray, horizontal bedding, σ_c=45 MPa
	3. sandy mudstone	22–24	20	dark gray, σ_c=36 MPa
	4. coal	1.15–1.45	1.3	semibright coal, fractured, σ_c=12 MPa
	5. mudstone	4–8	6.0	gray, horizontal laminated σ_c=30 MPa
	6. sandstone	16.0–24.0	18	gray, horizontal bedding, σ_c=60 MPa

(**a**)

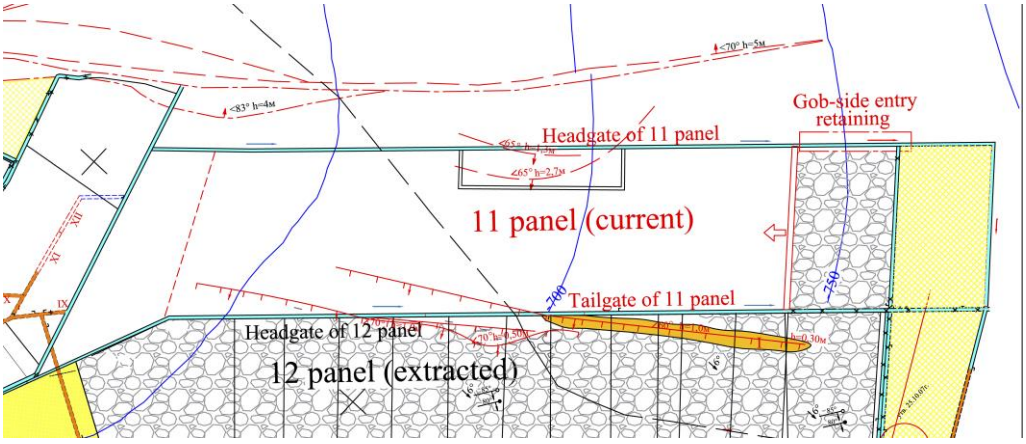

(**b**)

Figure 2. The geological and engineering conditions of a mine: (**a**) strata histogram; (**b**) layout of longwall panels.

2.2. Supporting Parameters and Deformation of Gob-Side Entry Retaining

A U-shaped steel arch support (U33) with steel mesh was used in the entry. The width and height of the entry were 5.2 m and 3.65 m, respectively. The cross-sectional area of the entry during the excavation stage was 15.1 m^2. The distance between the steel arch frames was 0.67 m. After coal mining in the longwall face, an artificial filling wall was built to maintain the gob-side entry. Figure 3a shows the original design of the support scheme. However, at a longwall retreat with a distance of 200 m, the width and height of the headgate of the 12-panel longwall were 2.6 m and 1.29 m, respectively. The total vertical convergence was about 64% of the initial roadway height. The average floor uplift was 1.04 m, and the average roof lowering was 1.32 m. The headgate deformed asymmetrically. The steel arches were critically bent and irreversibly deformed. The yielding nodes failed, and the steel mesh was disrupted. The entry required repair. The failure of the headgate support system and the floor heave consequences are shown in Figure 3b. To increase the load-bearing capacity of the steel arch frames, wooden pillars were installed. Floor restoration was carried out with a Hasemag EL160 loader machine to ensure the required cross-sectional area in the gob-side entry retaining. This practice is typical for coal mines in Ukraine [41]. Scholars from other countries report similar cases of critical floor heave [16,18,27,42,43].

Floor heave monitoring was performed in the headgate of the 12 panels. Measurements were carried out at three monitoring stations. The distance between stations was 9.6 m. Each station consisted of 4 marker points installed in the roof, floor, and both wall sides of the gateroad. The measurements were carried out over 4 months. The graphs of floor heave evolution in the center of the headgate span in front of the longwall face and behind it are presented in Figure 3c. The floor uplift in front of the longwall influence zone was 95 mm (9% of the total floor heave) and occurred during the roadway excavation stage. The monitoring results show that the main part of the floor uplift occurred at a distance of +40 m in front of the longwall face and −50 m behind it. In total, 35% of the floor uplift occurred at a distance of "+40" m in front of the longwall face to the intersection of the headgate with the face. Another 28% of floor uplift appears in the section of the headgate "0"–"−50" m behind the longwall face. The floor uplift has a damping tendency and stabilizes at a distance of 260–300 m behind the longwall face. At the stage of maintaining the headgate behind the longwall face, 56% of the total floor uplift occurs.

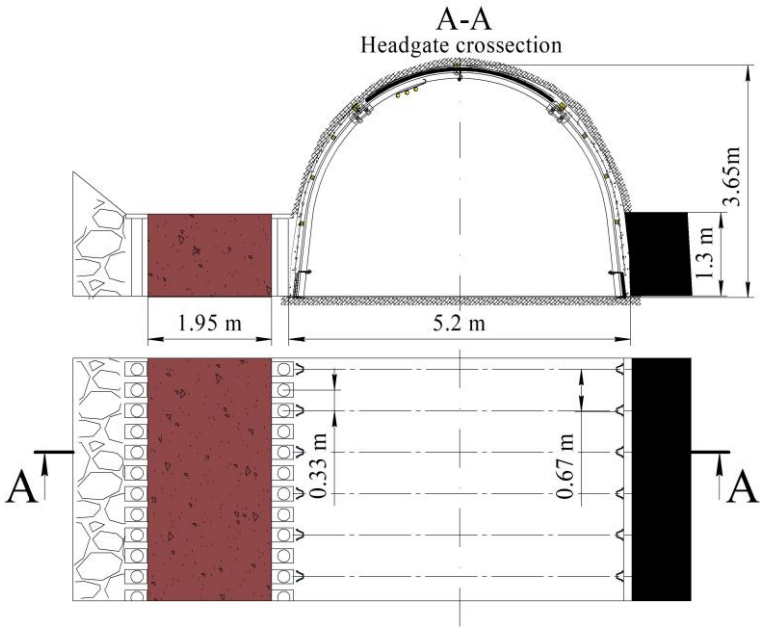

(**a**)

(**b**)

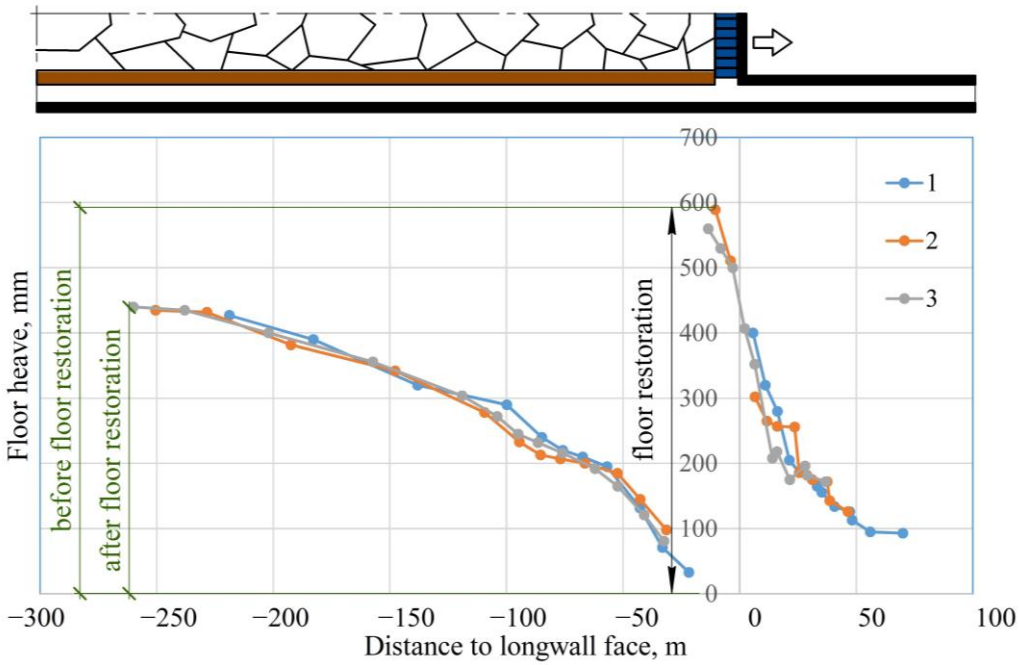

(**c**)

Figure 3. The parameters of the original support system (**a**), view on gob-side entry at a retreat of the longwall at a distance of 200 m (**b**), monitoring curve of floor heave in headgate in longwall face influence zone (**c**). 1, 2, 3—monitoring stations.

An analysis of the floor heave dynamic monitoring showed that this phenomenon evolved with different intensities at different stages of the gateroad's life. This is generally consistent with previous studies [15,17,27,41]. The gateroad that was an object of study had no water inflows. Therefore, the swelling mechanism of heaving is not typical for it. The greatest increase in gateroad floor heave was associated with the longwall face

influence. The abutment pressure changed the equilibrium state of rock masses, increased vertical stress concentration and led to post-elastic deformation of rocks. In this case, the immediate floor lost its continuity and became discontinued. This was visually confirmed after rock excavation during floor restoration, similar to previous studies [41]. Post-elastic deformation (pseudoplastic flow) and dilatancy are the main causes of floor heave. Floor heave in the gob-side entry is complicated by the asymmetrical stress–strain state. In this case, the heaving mechanism is close to bearing capacity in failure cases. However, due to the stress asymmetry, failures of the floor strata underneath the coal body and the filling wall body are different.

To control the lowering of the roof, the distance between the steel arch frames was reduced to 0.5 m in the gateroad of 11 panels. However, the floor of entry remained unsupported. So, the main problem for entry stability was the large floor heave. Floor restoration with dinting loaders is an ineffective passive method, which requires additional labor and material resources, organization of transport of the excavated rock, and time. Therefore, optimization of the support scheme to control floor heave is an important problem.

3. Study of the Floor Heave in Gob-Side Entry Retaining

3.1. Numerical Model

The geotechnical conditions of the 11-longwall panel of the Pivdennodonbasskaya coal mine were the basis of the numerical model that was realized by ANSYS 17.2 software. The simulation zone is indicated in Figure 4a, and the numerical model is shown in Figure 4b.

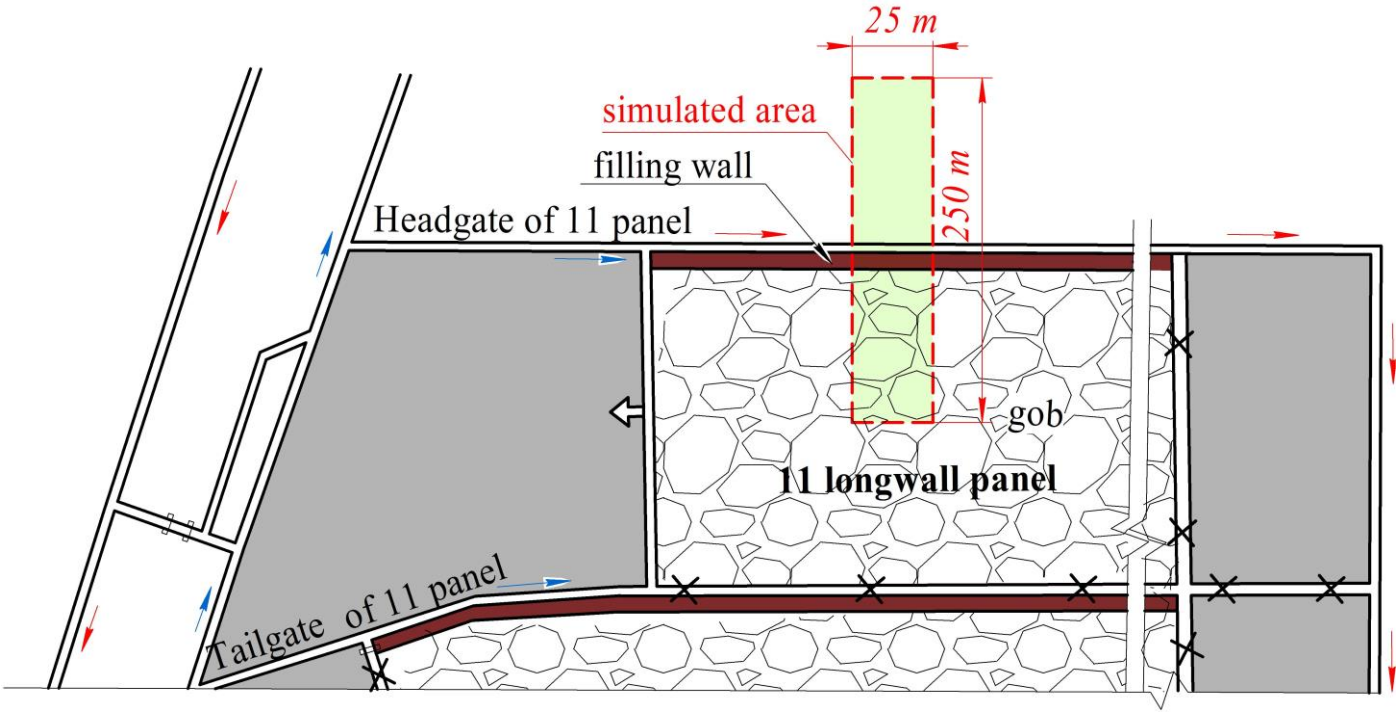

(**a**)

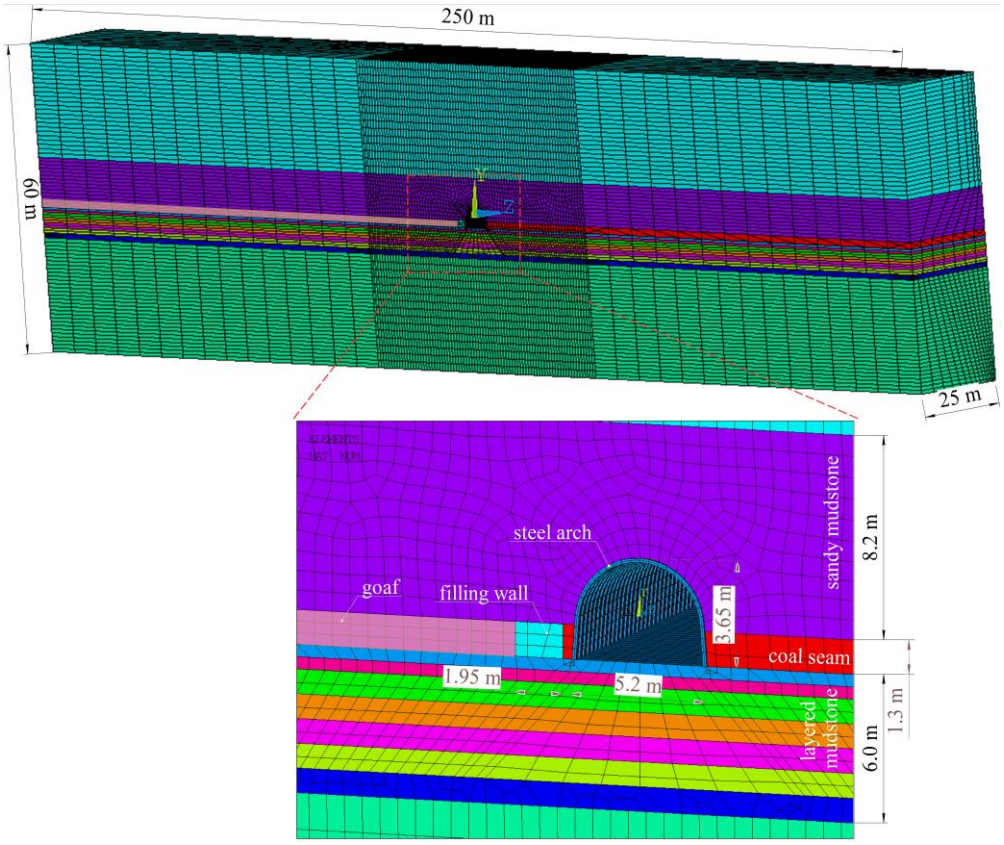

Figure 4. Plan of the simulated area (**a**); numerical model and support elements (**b**).

The model was three-dimensional (3D). The size is 250 m along the x direction, 60 m along the y direction, and 25 m along the z direction. Half of the panel width was simulated due to symmetry. The height and width of the gob-side entry were 3.65 m and 5.2 m, respectively. The height and width of the filling wall were 1.3 m and 1.95 m, respectively. The bottom boundary of the model was fixed vertically; displacements of lateral boundaries were constrained in the normal direction. Vertical pressure, which was equivalent to the strata weight at a depth of 900 m (22.5 MPa), was applied to the top boundary.

To simulate the behavior of rock mass, filling wall material, and gangue in the goaf, the Drucker–Prager model was applied. The capability of the Drucker–Prager model to adequately simulate the behavior of pressure-dependent materials (like rocks) has been shown in previous studies [44–46]. The bilinear isotropic hardening model was used to simulate the behavior of the steel arch frame, rock bolt, and steel pile.

The surrounding rocks of gob-side entry retaining were failured and discontinuous. Therefore, the mechanical parameters of intact rock (Figure 2a) should have been corrected. The Hoek–Brown Failure Criterion [47] was used to calculate the properties of rock mass in gob-side entry retaining. The Geological Strength Index (GSI), the "mi" constant, and the disturbance factor (D) were determined.

The GSI was calculated as RMR89-5 [48]. RMR89 was determined on the basis of geological documentation, results of the uniaxial strength tests, tests of the drill cores, and the observation of exposure of rock mass during gateroad repairs according to the Bieniawski method [49].

The "mi" constant was 8 for mudstones, 17 for coal, and 12 for sandstone. The D parameter corresponded to Hoek's classification categories: "squeezing problems result in significant floor heave, disturbance can be severe unless a temporary invert is placed"

for mudstone and sandstone; "mechanical excavation in poor quality rock masses resulting in minimal disturbance to the surrounding rock mass" for coal seams [47].

The deformation modulus (E_{rm}), friction angle (φ), and cohesive strength (c) were calculated according to Hoek and Diederichs' empirical method [48]. The calculation procedure was described in previous studies [18,50]. The calculated rock mass properties are presented in Table 1. The filling wall body in the case of a longwall retreat with a distance of 100 m was fissured and discontinuous. Therefore, the same method was applied for the filling wall material. The properties of the filling wall are shown in Table 1. To simulate the behavior of the broken gangue in the goaf, Poisson's ratio = 0.45, and E_{rm} = 30 MPa were applied [51]. The properties of the steel arch frame are shown in Table 2.

Table 1. Rock mass and filling wall material parameters for numerical simulation.

GSI	D	Compressive Strength (MPa)	Tensile Strength (MPa)	Deformation Modulus (GPa)	Poisson's Ratio	Cohesion Value (MPa)	Angle of Internal Friction (deg)	Dilatancy Angle (deg)
Main roof (sandy mudstone)								
52	0.5	1.75	0.09	1.19	0.3	2.83	24	24
Immediate roof (sandy mudstone)								
52	0.5	1.48	0.08	0.97	0.3	2.45	27	27
Coal seam c_{11}								
35	0	0.32	0.006	0.22	0.3	1.13	20	20
Immediate floor (mudstone)								
47	0.5	0.87	0.04	0.50	0.3	1.61	22	22
Main floor (sandstone)								
55	0.5	2.90	0.11	1.80	0.3	3.90	34	34
Filling wall material								
66	0.5	3.62	0.16	1.48	0.3	3.33	29	-

Table 2. Steel arch frame parameters for numerical simulation.

Primary Support	Type of Elements	Material Behavior Option	Elastic Modulus (GPa)	Poisson's Ratio	Yield Strength (MPa)	Tangent Modulus (GPa)
U-shaped steel support	Beam	Bilinear isotropic hardening	200	0.27	295	52.2

3.2. Simulation Results

The stress–strain distributions in the surrounding rocks are shown in Figures 5 and 6. The initial position of the rock layers during the excavation of the gateroad is shown in Figure 5a,b by the dashed line. In these figures, the movement of rock strata can be tracked comparative to the initial state. Specific displacements of rock strata are marked with arrows in Figure 5a. The subsidence of the roof above the longwall goaf, caused by coal mining, leads to loading of the filling wall body. As a result, the filling wall is pressed into the immediate floor, which causes an increase in the concentration of vertical stresses in it (Figure 5a). The magnitude of vertical pressure on the filling wall body depends on the length of the roof console above the goaf and the rigidity of the filling wall material [5]. This issue is not discussed in this paper.

From the side of the coal seam body, vertical stresses also increase in the roof and floor. Increased vertical stresses in the floor strata underneath the gateroad walls cause lateral expansion of rocks in the horizontal direction. Thus, the horizontal stresses in the

immediate floor underneath the filling wall and coal seam body increase. Moreover, the magnitude of these stresses underneath the filling wall is higher than underneath the coal seam body, as can be seen from Figure 5b. High horizontal stresses under the steel arch legs provoke transverse expansion of the rocks (in the vertical direction) and their displacement towards the gateroad cavity. This causes stress relief in the rock mass as it approaches the entry contour and changes stress sign in the near-contour area (Figure 5a,b). The zone of vertical rock expansion and elevation in the immediate floor covers 5 m in depth according to the numerical modeling results, which are shown in Figure 5b. As a result of the filling wall body indentation in the immediate floor underneath the wall, a zone of rock subsidence is formed, up to 3.5 m deep, as shown in Figure 5b. The floor heave was 948 mm. This is 9.7% lower than the results of in situ monitoring. Overall, it can be concluded that the numerical model is adequate.

The mechanism described above is confirmed by analyzing the strain distribution (Figure 5c,d).

The results of rock specimen tests show [52–55] that for mudstone, siltstone, argillite, and sandstone with a uniaxial strength of 25–40 MPa, the failure criterion for strain is about 0.02-0.03. Therefore, in the numerical simulation, the post-peak limit was accepted in the range of "−0.02"–"+0.02". In this paper, the authors do not study the failure of rocks in detail. The authors understand that in a triaxial stress field, failure will depend on the ratio of stress components and can vary. In the context of this study, it is important to recognize the post-elastic stage. Therefore, the post-peak strain is analyzed. In the Drucker–Prager model, pseudoplastic deformation is accepted for analyzing the behavior of rock mass beyond the elastic stage, including discontinuous rock.

The contour of the vertical expansion zone with post-peak strain is shown in Figure 5c. The positive strain scale in the figures is limited to "+0.05". All strains that are greater than +0.05 are indicated in gray. Vertical strains in this zone exceed the post-peak strain for mudstone by more than two times. In this zone, post-elastic deformation and delamination of rocks occur.

Zones of horizontal post-peak expansion of rocks are formed under the filling wall body and coal seam body. In these zones, dilatancy expansion of rock is observed under the influence of high vertical stresses (Figure 5d). The expansion of rocks in these zones leads to compression of the rocks between them, underneath the entry span. The post-peak horizontal compression zone is shown in Figure 5d. Dilatancy in this zone is caused by the horizontal stresses.

Zones of post-peak horizontal strains also form in the side walls of the entry. This causes deformation of the legs of the steel arch frame. The stress asymmetry not only leads to floor heave asymmetry but also irregular curvature of the support frame, which confirms the results of in situ observations in the gob-side entry retaining.

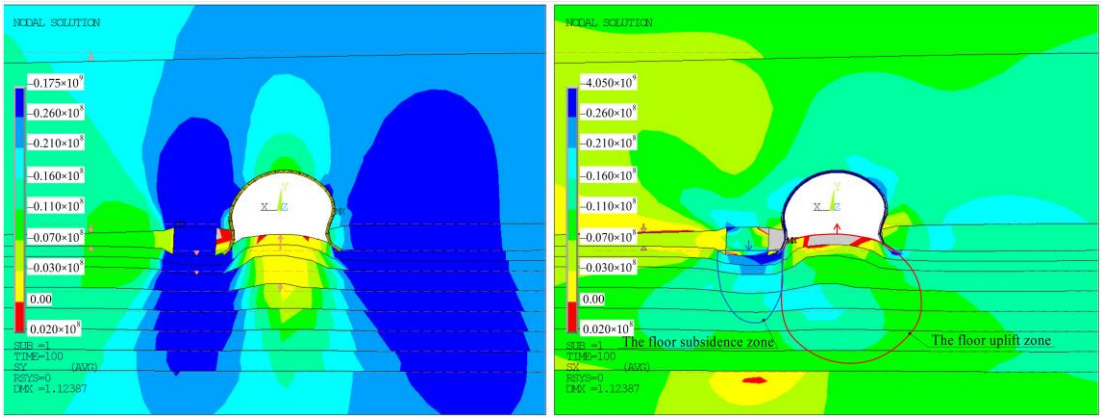

(**a**) (**b**)

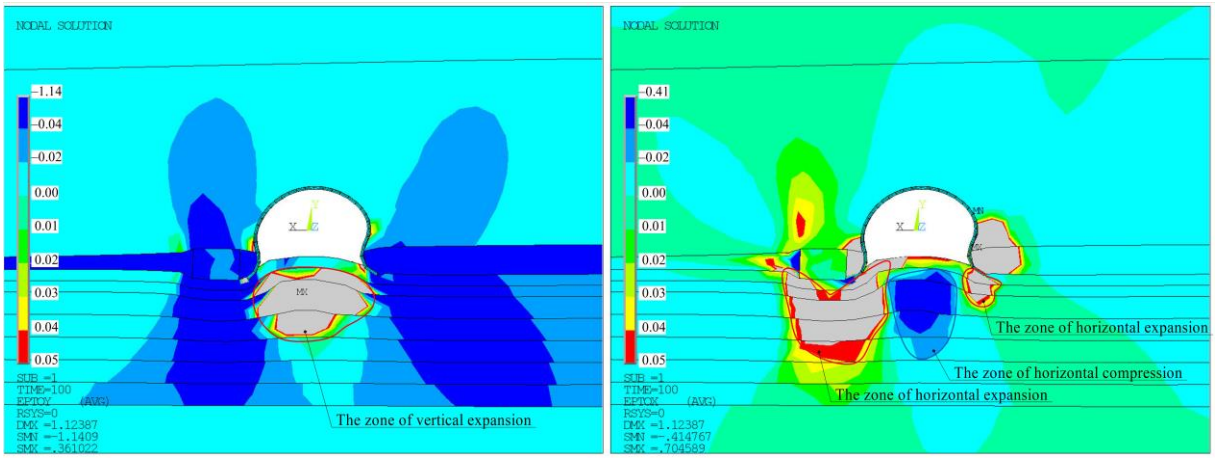

(**c**) (**d**)

Figure 5. Stress–strain distributions around the gob-side entry retaining: (**a**) vertical stress; (**b**) horizontal stress; (**c**) vertical strain; (**d**) horizontal strain.

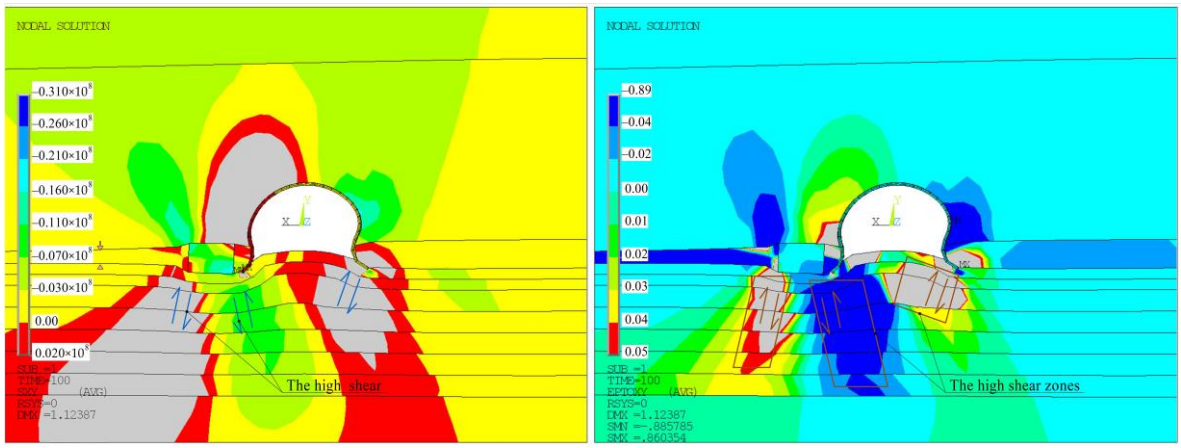

(**a**) (**b**)

Figure 6. Shear stress (a) and shear strain (**b**) distributions around the gob-side entry retaining.

Analysis of Figure 5 shows that counter-movements of rocks occur on the entry floor. Such movements cause shear deformations. Therefore, to analyze them, the distributions of shear stresses and strains in the surrounding rocks are shown in Figure 6. The main interest in this study is the central high-shear zone that occurs between the zone of uplift and the zone of subsidence of the immediate floor. This zone originates in the corner of the filling wall body and extends into the depth of the entry floor at an angle (Figure 6a). The post-peak shear strain zones are shown in Figure 6b. On the opposite side of the filling wall body and underneath the arch frame leg on the coal seam side, zones of increased shear stress and strain are also formed, as shown in Figure 6. Thus, shear has an important role in the deformation and failure of immediate floors.

The simulation results lead to comprehension of the floor heave mechanism in gob-side entry retaining. The main processes on the entry floor and their cause-and-effect relationships have been identified. The floor heave most likely corresponds to a buckling mechanism. Such findings are consistent with those reported by Mo et al. [22,27] regarding cases of floor heave in Australian mines. Since the main cause of heaving is horizontal stress, it can be concluded that a high degree of deformation is caused by rock mass buckling due to the failure of the floor materials in accordance with Mo et al.'s hypothesis [22].

3.3. Simulation Discussions

Several conclusions can be drawn according to the above analyses:

(1) The main reason for dramatic floor heave in gob-side entry retaining is the vertical loading of the filling wall by the weight of the roof that has lost its support after coal extraction in the longwall face. The high pressure of the roof leads to the indentation of the filling wall body into the immediate floor and the formation of a zone of increased vertical stresses underneath it. These stresses are higher than those on the side of the coal seam body, which is the main reason for the asymmetry of the gateroad deformation. Further redistribution of stresses in the immediate floor leads to an increase in horizontal stresses, which have a key role in floor heave.

(2) High vertical stresses underneath the filling wall and coal seam body lead to dilatancy expansion of rocks in the horizontal direction. High horizontal stresses in the immediate floor under the side wall provoke the formation of a post-peak horizontal compression zone under the entry span. In this zone, the dilatancy and lateral expansion of rocks in the vertical direction cause delamination of the immediate floor and uplift of discontinuous rocks.

(3) A zone of high shear occurs between the zone of rock uplift under the entry span and the zone of rock subsidence underneath the filling wall body. A zone of high shear stress and strain is also formed under the steel arch leg on the solid coal side. The rock failure in these zones complicates the floor heave mechanism described above. In shear strain zones, vertical stresses are transformed into horizontal ones.

(4) Numerical simulation results are valid only for geostress, geological and mechanical parameters of rock mass, filling wall setting, and support elements that were applied. However, the mechanism of floor heave is typical for similar engineering conditions.

4. Floor Heave Control with Anti-Shear Pile Technology

4.1. Design and Parameters of Floor Heave Control Schemes

The analysis of stresses and strains given in the previous section showed that the key factor of floor heave in gob-side entry retaining is the transmission of stresses from under the filling wall body to the zone under the entry span, which causes delamination, vertical expansion, and uplift of the discontinuous rocks in the immediate floor. A reinforcement method with anti-shear pile installation was proposed for the floor heave control.

The study of the effectiveness of the anti-shear pile was carried out in three stages. In the first stage, three floor heave control schemes with one anti-shear pile were studied. Each scheme was simulated twice: with a pile length of 2 m and 4 m. The distance between piles was equal to the distance between steel arch frames. Figure 7a–f show the support schemes that were studied. The parameters of the schemes are presented in Table 3.

In the second stage, three floor heave control schemes with two anti-shear piles were modeled. The length of each pile was 2.0 m. Thus, the summary pile length in the first simulation stage and in the second simulation stage was equal. Schemes of the second simulation stage are shown in Figure 7g–i.

In the third simulation stage, the investigation of the optimal type of pile was carried out. In this case, a comparison of three pile types was conducted:

- "Steel pile"—steel tube with a diameter of 200 mm and a wall thickness of 4 mm, filled with concrete (for this type of pile, two previous simulation stages were performed);
- "Steel tube"– steel tube with a diameter of 200 mm and a wall thickness of 4 mm;
- "Filling pile"—a pile of reinforced concrete (simulation was carried out for concrete classes B-20, B-40, and B-60).

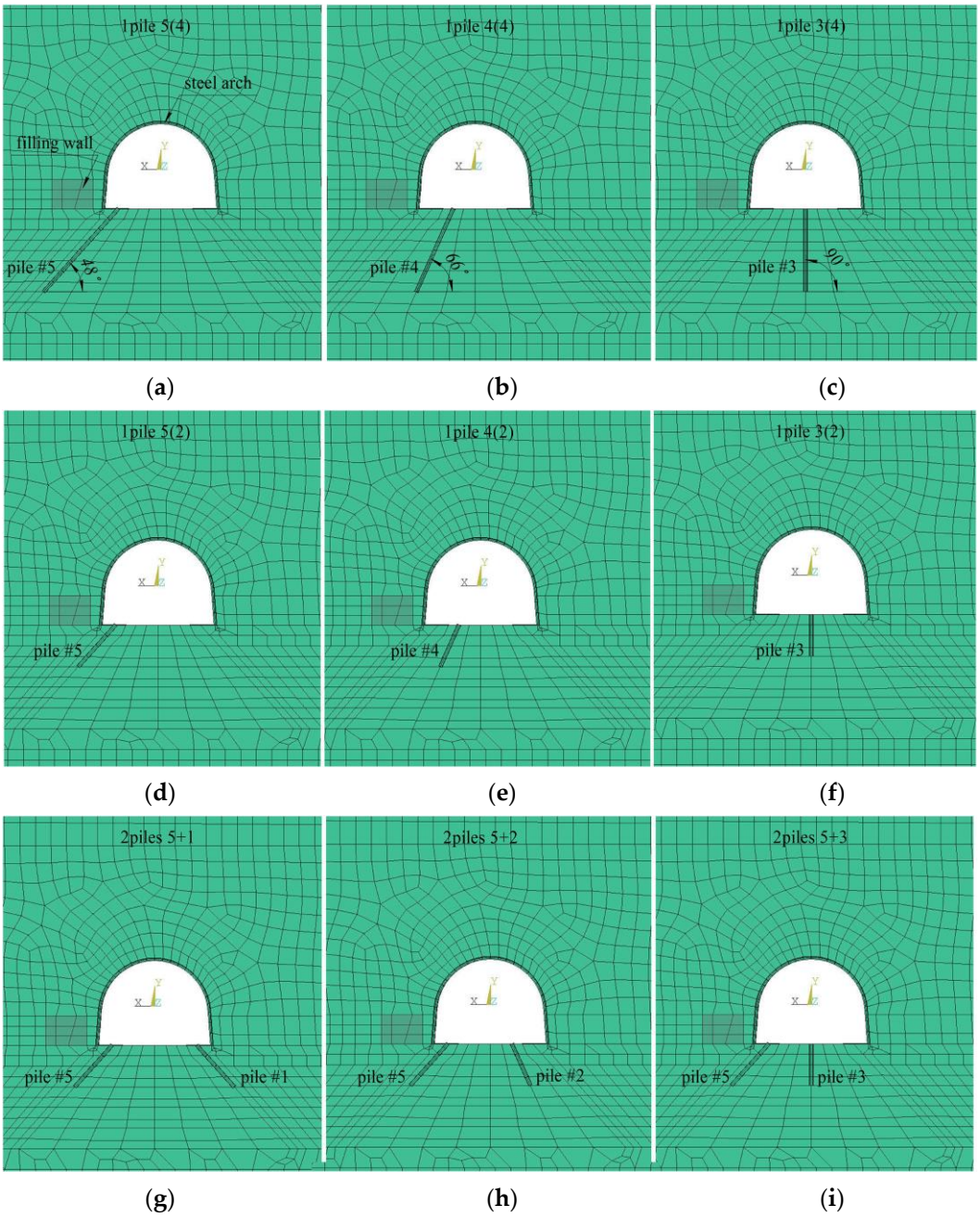

Figure 7. Finite-element models for simulated floor heave control schemes: (**a**) scheme 1pile 5 (4); (**b**) scheme 1pile 4 (4); (**c**) scheme 1pile 3 (4); (**d**) scheme 1pile 5 (2); (**e**) scheme 1pile 4 (2); (**f**) scheme 1pile 3 (2); (**g**) scheme 2pile 5+1; (**h**) scheme 2pile 5+2; (**i**) scheme 2pile 5+3.

The plan of the numerical experiment is presented in Table 3.

The pile positions were numbered in the direction from the solid coal body to the filling wall body. The central pile (position #3) has a vertical orientation along the axis of the roadway cross-section. The piles that were installed in floor corners (position #1, position #5) were inclined 48 degrees to the horizon. The piles in the position between the central pile and floor corner pile (position #2, position #4) were inclined 66 degrees to the horizon. The pile inclination was chosen by taking into account the simulation results presented in the previous section.

The original U-shaped steel arch was not changed. Table 3 shows the mechanical parameters of floor support components in the numerical model. The piles were modeled as beam elements. In this case, the deformation modulus was calculated as a weighted average

between steel and concrete for each pile type structure separately according to the theory of elasticity.

Table 3. The parameters of floor heave control schemes for numerical simulation.

Scheme	Number of Piles	Pile Position	Pile Length (m)	Summary Length of Piles (m)	Pile Type	Class Of Concrete in the Pile	Deformation Modulus (GPa)	Poisson's Ratio
1st simulation stage								
1pile 5 (4)	1	#5	4	4	Steel pile	B-60	72	0.25
1pile 4 (4)	1	#4	4	4	Steel pile	B-60	72	0.25
1pile 3 (4)	1	#3	4	4	Steel pile	B-60	72	0.25
1pile 5 (2)	1	#5	2	2	Steel pile	B-60	72	0.25
1pile 4 (2)	1	#4	2	2	Steel pile	B-60	72	0.25
1pile 3 (2)	1	#3	2	2	Steel pile	B-60	72	0.25
2nd simulation stage								
2pile 5+1	2	#5, #1	2	4	Steel pile	B-60	72	0.25
2pile 5+2	2	#5, #2	2	4	Steel pile	B-60	72	0.25
2pile 5+3	2	#5, #1	2	4	Steel pile	B-60	72	0.25
3rd simulation stage								
2pile 5+2	2	#5, #2	2	4	Steel pile	B-60	72	0.25
2pile 5+2(tube)	2	#5, #2	2	4	Steel tube	-	200	0.3
2pile 5+2(B-20)	2	#5, #2	2	4	Filling pile	B-20	27.5	0.19
2pile 5+2(B-40)	2	#5, #2	2	4	Filling pile	B-40	36.0	0.19
2pile 5+2(B-60)	2	#5, #2	2	4	Filling pile	B-60	39.5	0.19

4.2. Effectiveness of Anti-Shear Pile Method

First simulation stage.

In the first simulation stage, the search for the best floor control scheme was carried out while installing one pile.

The distributions of vertical strain and shear strain around the entry before and after pile installation are shown in Figures 8 and 9. It can be seen that the installation of the pile in any of the positions significantly reduces the size of the post-peak strain zone on the immediate floor. Pile installation does not significantly affect the distribution of compressive stresses; however, the zone of tensile stresses underneath the entry span is reduced. The smallest dimensions of this zone are for the 1pile 4 scheme (4) (Figure 8c). The pile installed in the entry corner (scheme 1pile 5 (4)) bends at a depth of 1–2 m in the zone of high horizontal stresses. This pile orientation effectively restricts floor delamination on the side of the filling wall, but practically does not restrain expansion on the side of the coal seam body (Figure 8b). Pile installation in the center of the entry span (scheme 1pile 3 (4)) restricts floor delamination on the side of the coal seam body, but on the side of the filling wall, vertical delamination remains significant (Figure 8d).

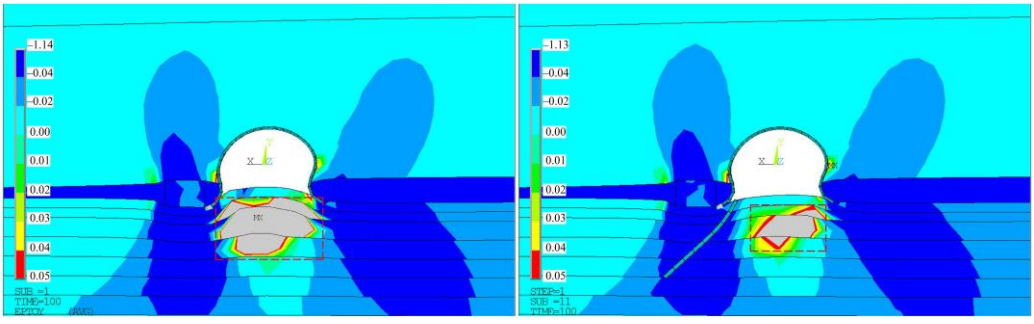

(**a**) (**b**)

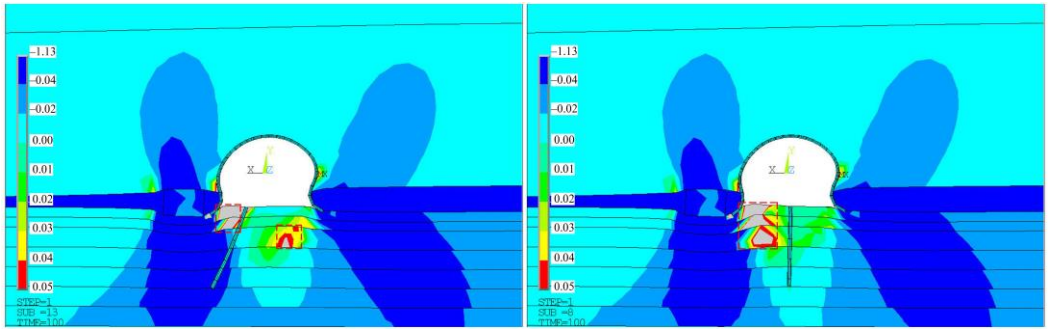

(**c**) (**d**)

Figure 8. The vertical strain distributions in surrounding rock in gob-side entry retaining: (**a**) before pile installation; after pile installation with schemes (**b**) 1pile 5 (4); (**c**) 1pile 4 (4); (**d**) 1pile 3 (4).

Pile installation has a similar effect on shear strain in the geometric sense. The smallest dimensions of the post-peak shear strain zone are for the 1pile 4 (4) scheme (Figure 9c). The pile in the center of the entry span (scheme 1pile 3 (4)) does not reduce the floor heave by the anti-shear (anti-slide) effect (Figures 8d and 9d). It is more likely that such pile installation halves the entry span, which ensures a reduction in floor delamination.

The discussed stress–strain distributions are in accordance with the results of the floor heave analysis. The floor heave before and after pile installation at the first simulation stage is shown in Figure 10a. The smallest contour uplifts among schemes with piles 4 m long are noted for the 1pile 4 (4) scheme. In this case, the smallest dimensions of the horizontal compression zone on the entry floor are observed (Figure 10b). However, the smallest dimensions of the horizontal post-peak expansion zone are observed in scheme 1pile 5 (4) (Figure 10b). This scheme is worthy of interest since the post-peak horizontal strain is the key factor of the floor heave in the gob-side entry, which was discussed in the previous section.

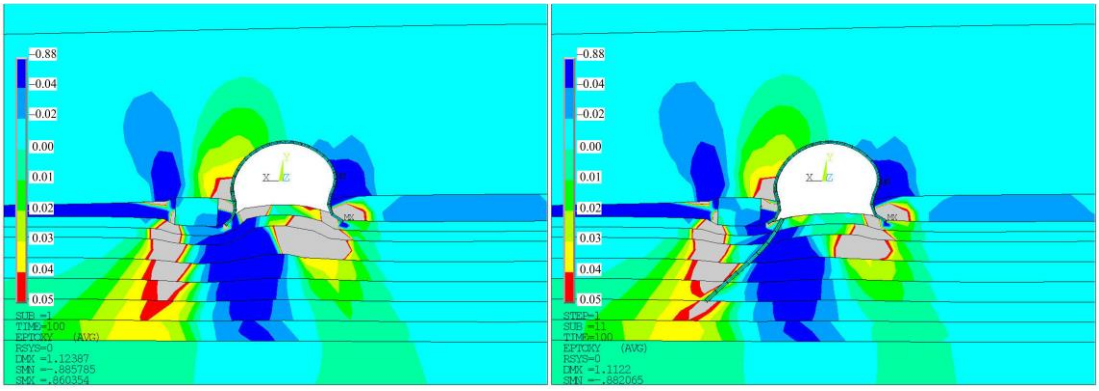

(**a**) (**b**)

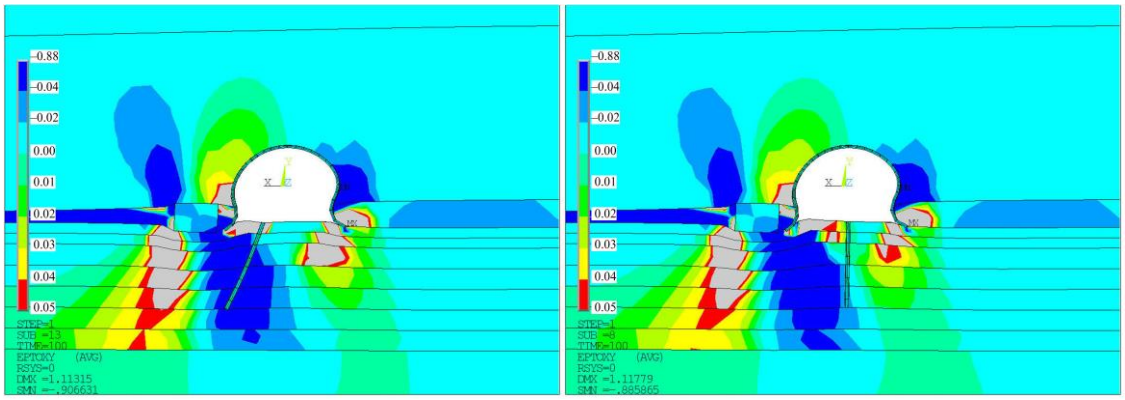

(**c**) (**d**)

Figure 9. The shear strain distributions in surrounding rock in gob-side entry retaining: (**a**) before pile installation; after pile installation with schemes (**b**) 1pile 5 (4); (**c**) 1pile 4 (4); (**d**) 1pile 3 (4).

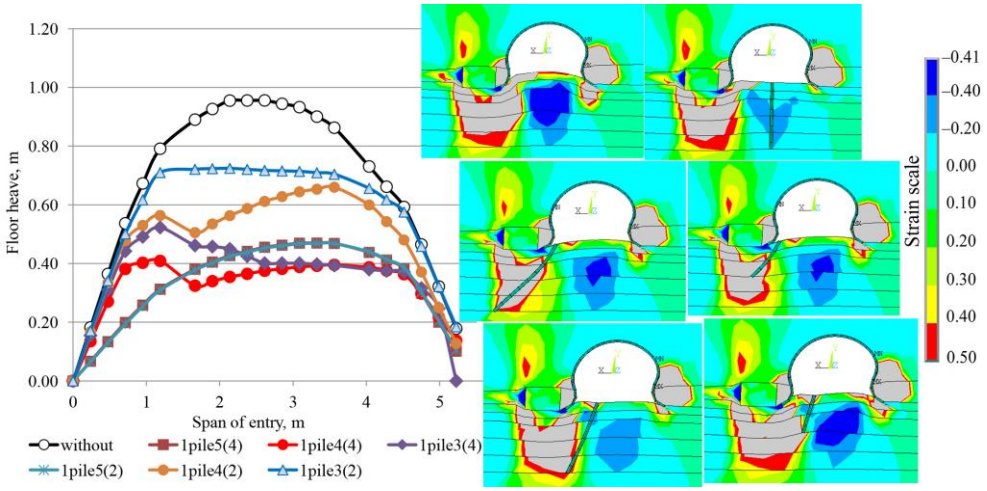

(**a**) (**b**)

Figure 10. The entry floor heave (**a**) and horizontal strain distributions in surrounding rock (**b**) before and after pile installation at the 1st simulation stage.

The vertical strain distributions around the gob-side entry retaining after installation of 2 m long piles are shown in Figure 11. Reducing the length of the piles to 2 m for schemes 1pile 4(2) and 1pile 3(2) led to a significant decrease in the efficiency of counteraction to immediate floor delamination. The 1pile 3(2) scheme affects only the local maximum of floor heave in the center of the entry (Figure 10a) and the vertical floor delamination in the central part of the entry span (Figure 11c). The size of the post-peak strain zone in the immediate floor does not decrease significantly compared to the case before pile installation (Figure 8a). Pile installation with the 1pile 4(2) scheme reduces the size of the vertical post-peak strain zone on the filling wall body side (Figure 11b), which leads to a decrease in floor heave on the filling wall side (Figure 10a). However, the length of the pile is insufficient to counteract the delamination of the floor from the side of the coal seam body (Figure 11b) and reduce the size of the horizontal expansion zones under the filling wall (Figure 10b). At the same time, the scheme 1pile 5(2) is as effective as the scheme 1pile 5(4). Reducing the pile length at this position does not have a significant effect on the floor heave (Figure 10a) and the configuration of the post-peak strain zones (Figure 11a, Figure 10b). The maximum floor heaves in the 1pile 4(4) and 1pile 5(2) schemes differ by only 60 mm, i.e., by 14%; at the same time, the pile length differs by 2.0 m, i.e., 50%. Therefore, it can be concluded that the 1pile 5(2) scheme is more effective.

The obtained results were the basis for the elaboration of schemes that were studied at the second simulation stage.

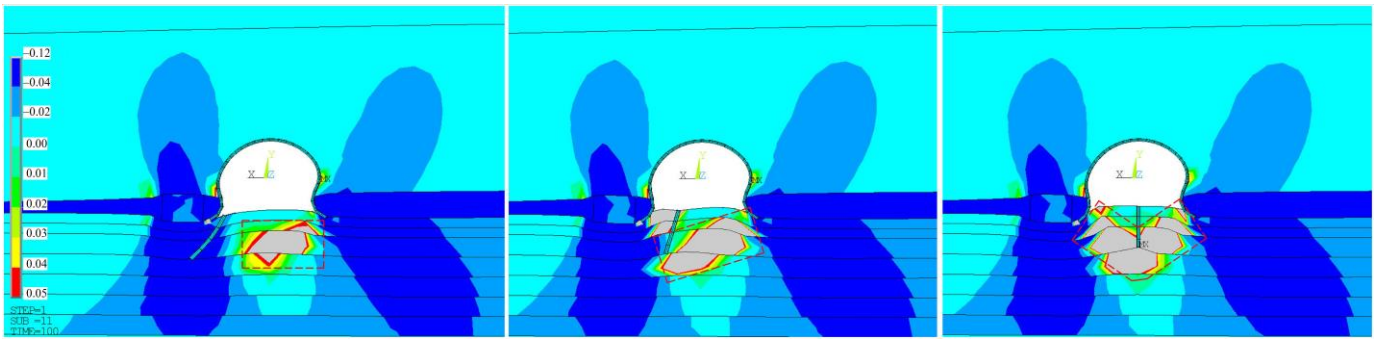

(**a**) (**b**) (**c**)

Figure 11. The vertical strain distributions around the gob-side entry retaining after pile installation with schemes (**a**) 1pile 5 (2); (**b**) 1pile 4 (2); (**c**) 1pile 3 (2).

Second simulation stage.

The elaboration of schemes for the second simulation stage was based on the concept that the summary length of the piles should not be more than 4.0 m (more than at the first simulation stage), since the borehole drilling and pile consumption depend on it. At this stage, it was assumed that two piles would be installed on the immediate floor. The position of one of these piles was determined in the results of the analysis of the investigation at the first simulation stage. This was position #5. Pile installation in this position leads to the highest efficiency among the compared ones. Thus, the most effective position for the second pile was searched for in the second simulation stage. The distributions of vertical strain and shear strain around the entry before and after pile installation are shown in Figures 12 and 13.

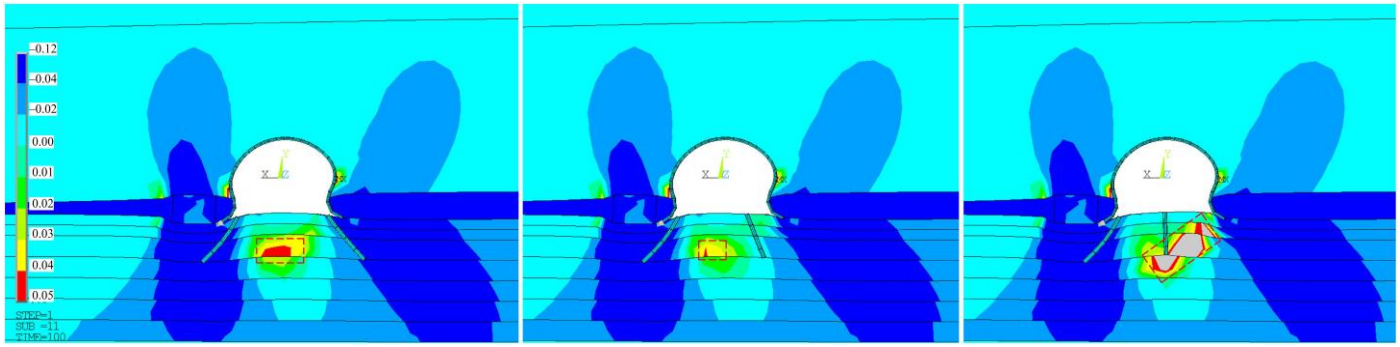

(**a**) (**b**) (**c**)

Figure 12. The vertical strain distributions around the gob-side entry retaining after pile installation with schemes (**a**) 2pile 5+1; (**b**) 2pile 5+2; (**c**) 2pile 5+3.

It can be seen that installing a second pile in any of the compared positions reduces the size of the post-peak strain zone on the immediate floor. The best effect is obtained in the case of the 2pile 5+2 scheme. The size of the vertical delamination zone (Figure 12b) and the post-peak shear strain zone (Figure 13b) is the smallest in this case. It is clear that this is reflected in the size of the floor heave, which is minimal for this scheme. The scheme 2pile 5+1 is less effective, as can be seen from the larger size of the post-peak shear strain (Figure 13a) and post-peak vertical strain (Figure 12a) on the entry floor. However, the 2pile 5+1 scheme is better than the scheme 2pile 5+3. The post-peak strain zones in the 2pile 5+3 scheme (Figures 12c and 13c) are the largest among the compared

schemes. It can be concluded that the anti-shear effect of pile installation is more efficient than the span-lowering effect for floor heave control in gob-side entry retaining.

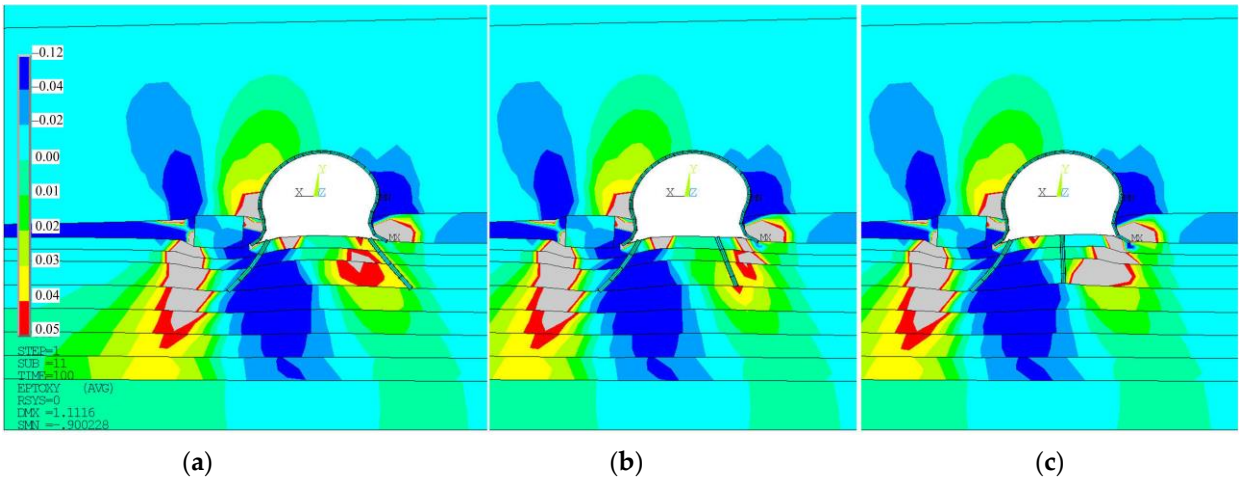

Figure 13. The shear strain distributions around the gob-side entry retaining after pile installation with schemes (**a**) 2pile 5+1; (**b**) 2pile 5+2; (**c**) 2pile 5+3.

The entry floor heave before and after pile installation at the second simulation stage is shown in Figure 14a. The scheme 2pile 5+2 is the most effective one. With this scheme, the maximum floor heave is 361 mm (Figure 14a), and the size of the horizontal post-peak strains is the smallest (Figure 14b). Thus, the most efficient scheme has been determined.

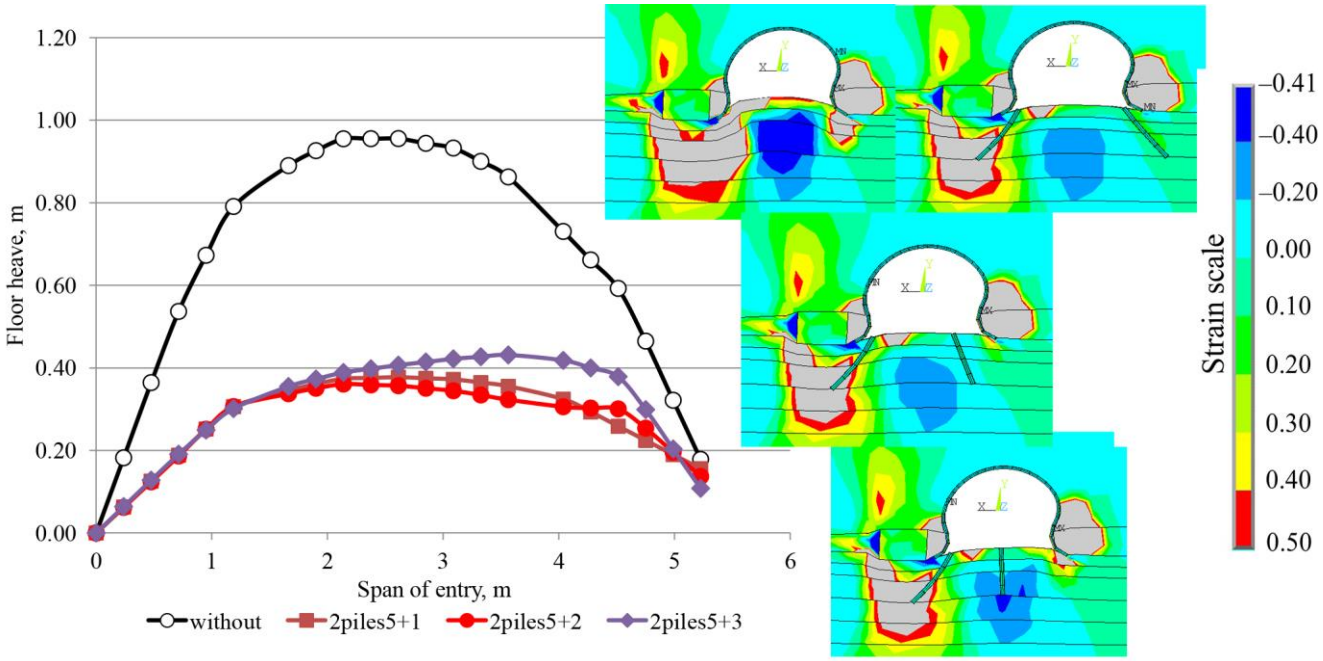

Figure 14. The entry floor heave and horizontal strain distributions in surrounding rock before and after pile installation at the 2nd simulation stage.

Third simulation stage.

For the practical implementation of the proposed method, it must satisfy two conditions: be technologically simple and inexpensive. There is no doubt that the piles should be installed in the gateroad outside the longwall influence zone. This will allow us to start floor heave control in a timely manner. Hole drilling for piles is a necessary process for floor support technology, and there is only one possible way to implement it.

Therefore, the attention at the third simulation stage was focused on finding the optimal type of pile. In order to find more economical and simple solutions, a technical and economic comparison of different types of piles was carried out. A metal tube with a concrete filling was the initial pile type, for which all previous simulation stages were carried out. This type of pile was called the "steel pile" (Figure 15a). As an alternative, pile variants were proposed, such as tubes without filling (scheme 2pile 5+2(tube)), called "steel tubes" (Figure 15b). Concrete filling piles with different concrete classes (2pile 5+2(B-20...B-60)) were also studied. In these piles, five main steel bars for longitudinal reinforcement and spiral lateral reinforcement stirrups were used (Figure 15c).

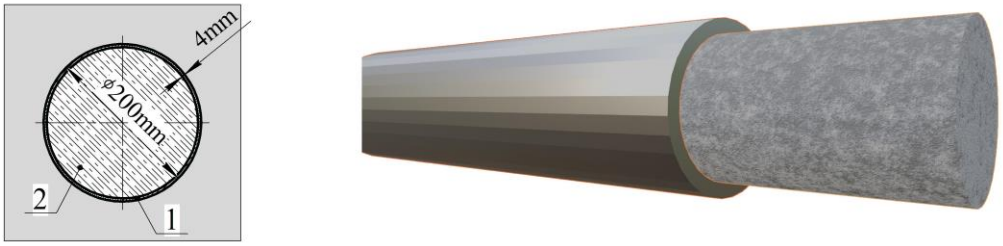

(**a**)

(**b**)

(**c**)

Figure 15. Pile design in numerical simulation: (**a**) steel pile; (**b**) steel tube; (**c**) filling pile. 1—steel tube (diameter 200 mm); 2—concrete; 3—main steel bars (5 × 14 mm); 4—lateral reinforcement stirrups (spiral length 14 m, diameter 6 mm).

The entry floor heave after pile installation with different schemes is shown in Figure 16. The form of the floor contour is the same for all pile variants. Steel piles have the best counteraction to heaving (the maximum floor heave is 361 mm). The worst variant is the "steel tube" (the maximum floor heave is 399 mm). The effectiveness of the "filling pile" depends on the class of concrete. Thus, the floor heave for the B-20 class is 397 mm, and for the B-60 class, it is 386 mm. An increase in the class of concrete leads to a decrease in the size of the vertical post-peak strain zone in the entry floor (Figure 17b,c) and a decrease in floor uplift. The localization and size of the post-peak strain zone for

the steel tube pile and filling pile with B-20 concrete do not differ (Figure 17a,b). However, the cost of piles varies significantly. A comparison of costs for one set of piles (2 × 2 m) for different types is shown in Table 4. The prices are correct for Ukraine as of March 2024.

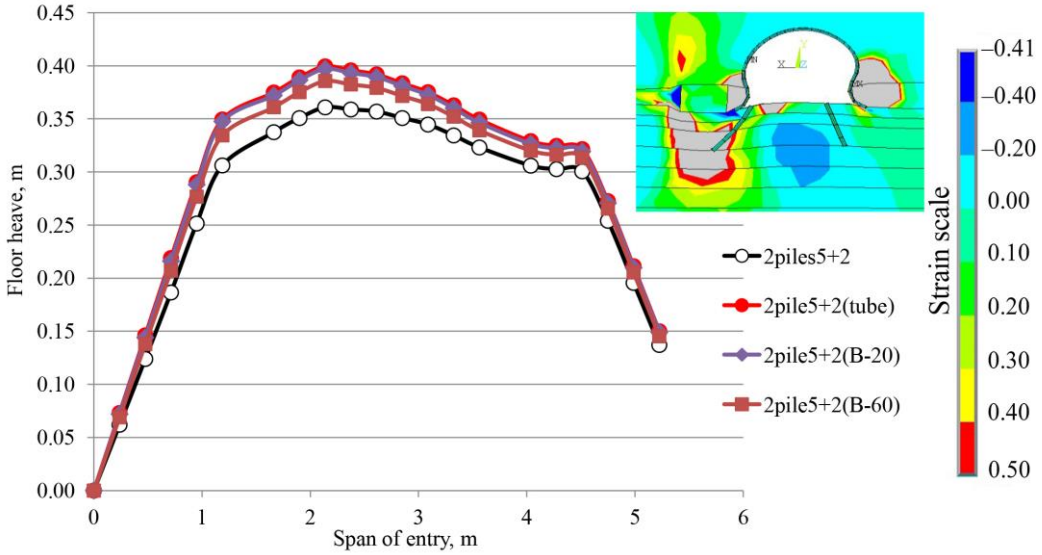

Figure 16. The entry floor heave after pile installation at the 3rd simulation stage with different schemes.

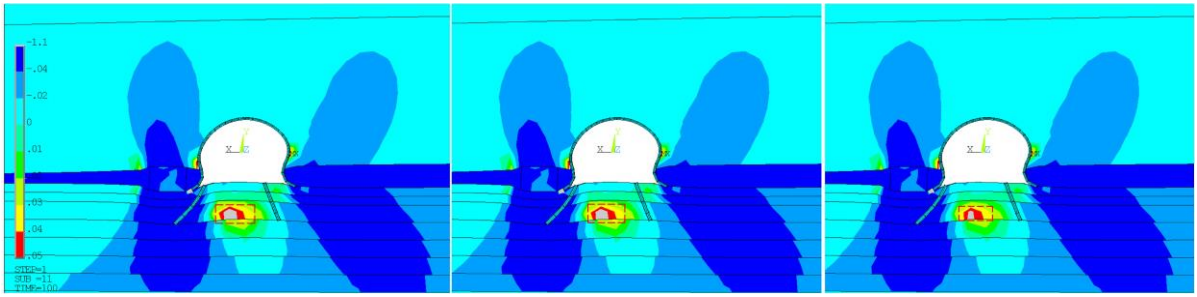

(**a**) (**b**) (**c**)

Figure 17. The vertical strain distributions around the gob-side entry retaining after pile installation with schemes (**a**) 2pile 5+2(tube); (**b**) 2pile 5+2(B-20); (**c**) 2pile 5+2(B-60).

Table 4. Comparison of the costs of materials for different types of piles with scheme 2pile 5+2.

Scheme	Pile Type	Class of Concrete in the Pile	Cost of Concrete, EUR	Cost of Tube, EUR	Cost of Longitudinal and Lateral Reinforcement, EUR	Total Cost, EUR	Maximal Floor Heave, mm
2pile 5+2	Steel pile	B-60	9.35	116.81		126.16	361
2pile 5+2 (tube)	Steel tube	-	-	116.81		116.81	399
2pile 5+2 (B-20)	Filling pile	B-20	8.48	-	25.92	34.40	397
2pile 5+2 (B-40)	Filling pile	B-40	8.78	-	25.92	34.70	389
2pile 5+2 (B-60)	Filling pile	B-60	9.35	-	25.92	35.27	386

Filling piles have a minimal cost, which gives them an advantage. So, with the 2pile 5+2(B-60) scheme, the cost of the pile is 3.57 times less than with the 2pile 5+2 scheme. Installation of the filling pile is easier, since the weight of reinforcement elements is less, which also reduces transportation costs. In addition, the installation of reinforcement of filling piles, unlike the installation of tubes, can be carried out without significant labor

costs. Thus, filling piles are more beneficial for floor heave control. The design of the proposed pile is shown in Figure 15c. Optimization of pile reinforcement design requires additional research and is not studied in this article.

4.3. Filling Pile Floor Support Scheme

The analysis of monitoring of gob-side entry retaining shows that the main gateroad stability problem is dramatic floor heave. Therefore, the modification of the current support system of the entry is necessary.

Based on numerical simulation results, it was found that the most effective floor support scheme is the 2pile 5+2 (B-60) scheme. Additional installation of piles in the original support system was proposed. The rationale for the effectiveness of this scheme is presented in the previous section of this paper. Figure 18 shows the proposed design of the support scheme. Drilling of boreholes for piles into the entry floor can be carried out with a machine for drilling degassing wells. SBG-1M is an example of such a machine.

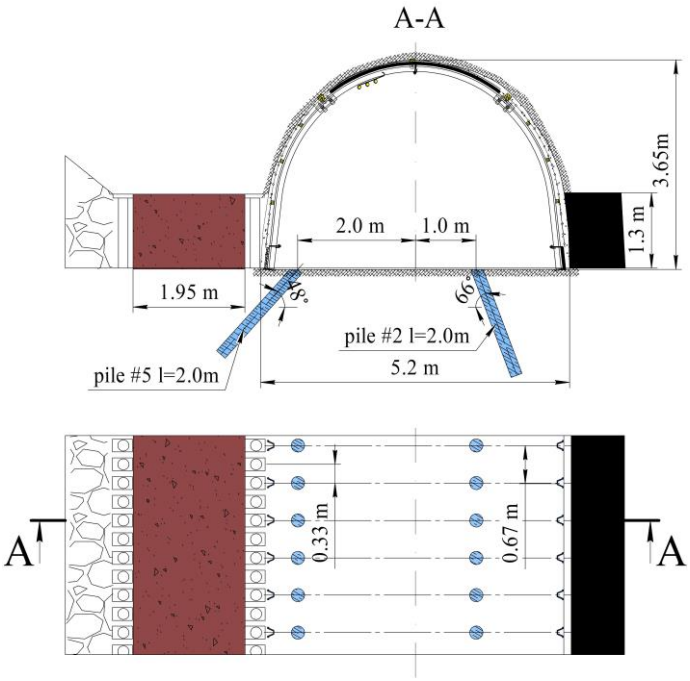

Figure 18. Design of support scheme.

According to the authors, the proposed anti-shear pile technology does not require significant investment. Investments are required to purchase an SBG-1M-type drilling machine. The approximate cost of such equipment in Ukraine, taking into account transportation costs, is EUR 15,000. Taking into account the service life, residual value, average monthly depreciation, and downtime, the depreciation expense will be EUR 205/month. The machine repairs and maintenance expenses, taking into account planned repairs, are 0.012 man-hours. Taking into account wages in Ukraine, monthly maintenance expenses will be EUR 119/month. Electric energy consumption and the salary of a worker operating the drilling machine depend on local wages and the quantities of drilling work. Three workers per shift are involved in the implementation of the proposed technology.

Pile installation must be carried out after the roadway excavation stage, and before the longwall mining stage. Therefore, the production schedule of the working face does not affect the schedule of pile installation. The estimated pace of installation of piles in a gateroad in a three-shift operating mode is 819 m/month.

5. Conclusions

This study was focused on floor heave evolution and its restriction in gob-side entry retaining. Floor heave control with anti-shear pile technology was studied. Numerical simulation by ANSYS 17.2 software was used for the stress–strain analysis of the surrounding rock. As a result, a floor heave mechanism was proposed. Based on the analysis of the floor heave causes, perspective schemes for immediate floor reinforcement were proposed and a study of their effectiveness was conducted. Based on the results of this investigation, the following conclusions can be drawn:

(1) The transformation of high vertical stresses, which arise in the entry floor underneath the filling wall and coal seam body, into horizontal stresses starts the floor heave process. Increased vertical stresses under the filling wall and coal seam body cause the dilatancy expansion of rocks in the horizontal direction. As a result, a zone of horizontal compression underneath the entry span occurs. Rocks within this zone, in the process of dilatancy expansion to relieve stress, displace towards the entry cavity. This leads to the delamination of rocks in the vertical direction and uplift of the entry contour. Between the zone of rock uplift under the entry span and the zones of rock subsidence underneath the filling wall body and coal seam body, high-shear zones arise, in which vertical stresses are transformed into horizontal ones. The rock failure in these zones complicates the floor heave mechanism described above.

(2) The ways to control floor heave are (1) restricting stress transformation in the entry floor; (2) increasing the bearing capacity of the immediate floor to counteract rock dilatation and delamination. A floor heave control method with anti-shear pile installation was proposed. The numerical simulation results confirmed the efficiency of pile installation. This makes it possible to significantly reduce the floor heave and the size of the zone of horizontal post-peak strain. As a result of numerical simulation, the most effective scheme (2pile 5+2) was found. A technical and economic comparison of different types of piles was carried out to find the most economical and simple solutions for the practical implementation of this scheme. Analysis of the numerical simulation results and the cost comparison of different types of piles shows that filling piles are the most effective ones. The cost of filling piles is more than 3.5 times less than the steel pile cost. In addition, the installation of filling piles does not require significant labor costs; the weight of the reinforcement used in this scheme is less than the weight of tubes in analog piles, which also reduces transportation costs. The implementation of the proposed floor heave control method with anti-shear piles leads to a significant reduction in heaving in gob-side entry retaining. The results of this study can be used to design a support system in gob-side entry retaining.

(3) Anti-shear pile technology is at the stage of elaboration and justification of parameters. In situ tests are planned for the future. Therefore, the above-described effect is based only on the results of numerical simulation so far. Further research will aim to study the effectiveness of the proposed floor heave control method in situ in coal mines. The best design for filling piles will also be found.

Author Contributions: Conceptualization, I.S. and S.S.; methodology, I.S. and O.I.; software, I.S. and K.S.; validation, I.S., K.S., K.Z., and A.Z.; formal analysis, S.S.; investigation, I.S.; resources, K.Z. and A.Z.; writing—original draft preparation, I.S.; writing—review and editing, K.S. and S.S.; visualization, O.I.; supervision, I.S.; project administration, I.S.; funding acquisition, K.S., K.Z., and A.Z. All authors have read and agreed to the published version of the manuscript.

Funding: This research received no external funding.

Data Availability Statement: The original contributions presented in this study are included in the article; further inquiries can be directed to the corresponding author.

Acknowledgments: The authors are grateful to the administration of Donetsk National Technical University and AGH University of Science and Technology for supporting this research.

Conflicts of Interest: The authors declare no conflicts of interest.

References

1. Yang, X.; Huang, R.; Yang, G.; Wang, Y.; Cao, J.; Liu, J.; He, M. Validation study of no-pillar mining method without advance tunneling: A case study of a mine in China. *Energy Sci. Eng*. **2021**, *9*, 1761–1772. https://doi.org/10.1002/ese3.949.
2. He, M.; Wang, Q.; Wu, Q. Innovation and future of mining rock mechanics. *J. Rock Mech. Geotech. Eng*. **2021**, *13*, 1–21. https://doi.org/10.1016/j.jrmge.2020.11.005.
3. Chen, A. Width Design of Small Coal Pillar of Gob-Side Entry Driving in Soft Rock Working Face and Its Application of Zaoquan Coal Mine. *Adv. Civ. Eng*. **2021**, *2021*, 9999957. https://doi.org/10.1155/2021/9999957.
4. Wang, D.; Li, S.; Wang, Q.; Li, W.; Wang, F.; Wang, H.; Peng, P.; Ruan, G. Experimental study of reasonable coal pillar width in fully mechanized top coal caving face of deep thick coal seam. *Chin. J. Rock Mech. Eng*. **2014**, *33*, 539–548.
5. Sakhno, I.; Sakhno, S.; Kamenets, V. Stress environment around head entries with pillarless gobside entry retaining through numerical simulation incorporating the two type of filling wall. *IOP Conf. Ser. Earth Env. Sci*. **2022**, *1049*, 012011. https://doi.org/10.1088/1755-1315/1049/1/012011.
6. Xie, S.R.; Wang, E.; Chen, D.D.; Li, H.; Jiang, Z.S.; Yang, H.Z. Stability analysis and control technology of gob-side entry retaining with double roadways by flling with high-water material in gently inclined coal seam. *Int. J. Coal Sci. Technol.* **2022**, *9*, 52. https://doi.org/10.1007/s40789-022-00524-x.
7. Ning, J.; Wang, J.; Bu, T.; Hu, S.; Liu, X. An innovative support structure for gob-side entry retention in steep coal seam mining. *Minerals* **2017**, *7*, 75. https://doi.org/10.3390/min7050075.
8. Kong, D.; Pu, S.; Cheng, Z.; Wu, G.; Liu, Y. Coordinated Deformation Mechanism of the Top Coal and Filling Body of Gob-Side Entry Retaining in a Fully Mechanized Caving Face. *Int. J. Geomech.* **2021**, *21*, 04021030. https://doi.org/10.1061/(ASCE)GM.1943-5622.000197.
9. He, M.; Song, S.; Wang, Q.; Yang, H.; Qi, H.; Guo, Z. Theory of longwall mining by using roof cuting shortwall team and 110 method—The third mining science and technology reform. *Coal Sci. Technol. Mag.* **2017**, *1*, 13. https://doi.org/10.19896/j.cnki.mtkj.2017.01.002.
10. Wang, M.; Xu, Y.L.; Xu, Q.Y.; Shan, C.F.; Li, Z.H.; Nan, H.; Li, Y.F.; Liu, H.L.; Chu, T.X. Stability control of overburden and coal pillars in the gob-side entry under dynamic pressure. *Int. J. Rock Mech. Min. Sci.* **2023**, *170*, 105490.
11. Zhang, Z.; Shimada, H.; Sasaoka, T.; Hamanaka, A. Stability Control of Retained Goaf-Side Gateroad under Different Roof Conditions in Deep Underground Y Type Longwall Mining. *Sustainability* **2017**, *9*, 1671.
12. Hu, J.; He, M.; Wang, J.; Ma, Z.; Wang, Y.; Zhang, X. Key Parameters of Roof Cutting of Gob-Side Entry Retaining in a Deep Inclined Thick Coal Seam with Hard Roof. *Energies* **2019**, *12*, 934. https://doi.org/10.3390/en12050934.
13. Xu, Y.; Chen, J.; Bai, J. Control of floor heaves with steel pile ingob-side entry retaining. *Int. J. Min. Sci. Technol.* **2016**, *26*, 527–534. https://doi.org/10.1016/j.ijmst.2016.02.024.
14. Hao, J.; Zhang, P.; Song, Y.; Liu, H.; Shi, Y.; Liu, J.; Lu, G. Research on Pillarless Mining by Gob-Side Caving under Soft Rock Roof Conditions: A Case Study. *Appl. Sci.* **2023**, *13*, 2816. https://doi.org/10.3390/app13052816.
15. Gong, P.; Ma, Z.; Ni, X.; Zhang, R.R. Floor heave mechanism of gob-side entry retaining with fully-mechanized backfilling mining. *Energies* **2017**, *10*, 2085. https://doi.org/10.3390/en10122085.
16. Li, Z.; Zhang, Y.; Ma, Q.; Zheng, Y.; Song, G.; Yan, W.; Zhang, Y.; Hu, L. The floor heave mechanism and control technology of gob-side entry retaining of soft rock floor. *Sustainability* **2023**, *15*, 6074. https://doi.org/10.3390/su15076074.
17. Yu, G.; Wang, J.; Hu, J.; Zhu, D.; Sun, H.; Ma, X.; Ming, W.; Li, W. Innovative control technique for the floor heave in goaf-side entry retaining based on pressure relief by roof cutting. *Math. Probl. Eng.* **2021**, *2021*, 7163598. https://doi.org/10.1155/2021/7163598.
18. Małkowski, P.; Ostrowski, Ł.; Stasica, J. Modeling of floor heave in underground roadways in dry and waterlogged conditions. *Energies* **2022**, *15*, 4340. https://doi.org/10.3390/en15124340.
19. Li, C.; Zuo, J.; Chunchan, W.; Xu, X. Fracture Development at Laminated Floor Layers Under Longwall Face in Deep Coal Mining. *Nat. Resour. Res*. **2020**, *29*, 3857–3871. https://doi.org/10.1007/s11053-020-09684-6.
20. Guo, G.; Kang, H.; Qian, D.; Gao, F.; Wang, Y. Mechanism for Controlling Floor Heave of Mining Roadways Using Reinforcing Roof and Sidewalls in Underground Coal Mine. *Sustainability* **2018**, *10*, 1413. https://doi.org/10.3390/su10051413.
21. Kang, Y.; Liu, Q.; Gong, G.; Wang, H. Application of a combined support system to the weak floor reinforcement in deep underground coal mine. *Int. J. Rock Mech. Min. Sci*. **2014**, *71*, 143–150. https://doi.org/10.1016/j.ijrmms.2014.03.017.
22. Mo, S.; Ramandi, H.L.; Oh, J.; Masoumi, H.; Canbulat, I.; Hebblewhite, B.; Saydam, S. A new coal mine floor rating system and its application to assess the potential of floor heave. *Int. J. Rock Mech. Min*. **2020**, *128*, 104241. https://doi.org/10.1016/j.ijrmms.2020.104241.
23. Zhang, Z.Y.; Shimada, H. Numerical study on the effectiveness of grouting reinforcement on the large heaving floor of the deep retained goaf-side gateroad: A case study in China. *Energies* **2018**, *11*, 1001. https://doi.org/10.3390/en11041001.
24. Chen, Y.; Bai, J.B.; Yan, S.; Xu, Y.; Wang, X.Y.; Ma, S. Control mechanism and technique of floor heave with reinforcing solid coal side and floor corner in gob-side coal entry retaining. *Int. J. Min. Sci. Technol.* **2012**, *22*, 841–845. https://doi.org/10.1016/j.ijmst.2012.12.002.
25. Gao, F.; Stead, D.; Kang, H.; Wu, Y. Discrete element modelling of deformation and damage of a roadway driven along an unstable goaf—A case study. *Int. J. Coal Geol.* **2014**, *127*, 100–110. https://doi.org/10.1016/j.coal.2014.02.010.
26. Faria Santos, C.; Bieniawski, Z.T. Floor design in underground coal mines. *Rock Mech. Rock Eng.* **1989**, *22*, 249–271.

27. Mo, S.; Sheffield, P.; Corbett, P.; Ramandi, H.L.; Oh, J.; Canbulat, I.; Saydam, S. A numerical investigation into floor buckling mechanisms in underground coal mine roadways. *Tunn. Undergr. Space Technol.* **2020**, *103*, 103497. https://doi.org/10.1016/j.tust.2020.103497.
28. Zhai, W.; He, F.; Xu, X.; Lv, K.; Li, L.; Song, J. Floor heave mechanism in water-rich soft rock roadways and a DS-IBA control approach. *Geomat. Nat. Hazards Risk* **2022**, *13*, 2107–2123. https://doi.org/10.1080/19475705.2022.2107439.
29. Wang, C.; Chen, X.Y.; Zhang, J.D.; Wu, Y.P. Stability Mechanism and Repair Method of U-Shaped Steel Reverse Arch Support in Soft Floor Roadway. *Adv. Civ. Eng.* **2020**, *2020*, 8814365. https://doi.org/10.1155/2020/8814365.
30. Zheng, W.; Zhao, Y.; Bu, Q. The coupled control of floor heave based on a composite structure consisting of bolts and concrete antiarches. *Math. Probl. Eng.* **2018**, *2018*, 3545423. https://doi.org/10.1155/2018/3545423.
31. Zhai, X.X.; Qin, L.T.; Chen, C.Y. Combined Supporting Technology of Anchoring and Grouting and Floor Relief in Deep Chamber of Belt Conveyor. *Chin. J. Undergr. Space Eng.* **2017**, *5*, 1363–1372. https://doi.org/10.3390/en11010067.
32. Zhu, L.; Liu, C.; Gu, W.; Yuan, C.; Wu, Y.; Liu, Z.; Song, T.; Sheng, F. Research on Floor Heave Mechanisms and Control Technology for Deep Dynamic Pressure Roadways. *Processes* **2023**, *11*, 467. https://doi.org/10.3390/pr11020467.
33. Wang, D.; Zheng, Y.; He, F.; Song, J.; Zhang, J.; Wu, Y.; Jia, P.; Wang, X.; Liu, B.; Wang, F.; et al. Mechanism and Control of Asymmetric Floor Heave in the Gob-Side Coal Roadway under Mining Pressure in Extra-Thick Coal Seams. *Energies* **2023**, *16*, 4948. https://doi.org/10.3390/en16134948.
34. Wei, W.; Zhang, G.; Li, C.; Zhang, W.; Shen, Y. Mechanism and Control of Asymmetric Floor Heave in Deep Roadway Disturbed by Roof Fracture. *Sustainability* **2023**, *15*, 6357. https://doi.org/10.3390/su15086357.
35. Zhang, D.; Bai, J.; Yan, S.; Wang, R.; Meng, N.; Wang, G. Investigation on the Failure Mechanism of Weak Floors in Deep and High-Stress Roadway and the Corresponding Control Technology. *Minerals* **2021**, *11*, 1408. https://doi.org/10.3390/min11121408.
36. Qin, D.; Wang, X.; Zhang, D.; Chen, X. Study on Surrounding Rock-Bearing Structure and Associated Control Mechanism of Deep Soft Rock Roadway Under Dynamic Pressure. *Sustainability* **2019**, *11*, 1892. https://doi.org/10.3390/su11071892.
37. Kang, H.; Wang, J.; Lin, J. Case studies of rock bolting in coal mine roadways. *Chin. J. Rock Mech. Eng.* **2010**, *29*, 649–664.
38. Yang, J.; Shi, H.; Gan, Q.I. Research on mechanism for floor heave control in the roadway by base-angel-bolt and its type selection test. *J. Min. Saf. Eng.* **2016**, *33*, 643–648.
39. Kang, X.; Guo, D.; Lu, Z. Mechanism of roadway floorheave controlled by floor corner pile in deep roadway underhigh horizontal stress. *Adv. Civ. Eng.* **2021**, *2021*, 6669233. https://doi.org/10.1155/2021/6669233.
40. Guo, D.; Kang, X.; Lu, Z.; Chen, Q. Mechanism and Control of Roadway Floor Rock Burst Induced by High Horizontal Stress. *Shock Vib.* **2021**, *2021*, 6745930. https://doi.org/10.1155/2021/6745930.
41. Sakhno, I.; Isayenkov, O.; Rodzin, S. Local reinforcing of footing supported in the destroyed rock massif. *Min. Miner. Depos.* **2017**, *11*, 9–16. https://doi.org/10.15407/mining11.01.009.
42. Małkowski, P.; Ostrowski, Ł.; Bednarek, Ł. The effect of selected factors on floor upheaval in roadways-in situ testing. *Energies* **2020**, *13*, 5686. https://doi.org/10.3390/en13215686.
43. Liu, H.; Zhang, B.; Li, X.; Liu, C.; Wang, C.; Wang, F.; Chen, D. Research on roof damage mechanism and control technology of gob-side entry retaining under close distance gob. *Eng. Fail. Anal.* **2022**, *138*, 106331. https://doi.org/10.1016/j.engfailanal.2022.106331.
44. Liu, Q.; Fu, Q.; Yang, K.; Wei, Q.; Liu, H.; Wu, H. Geomechanical Modeling and Inversion Analysis of the *in-situ* Stress Field in Deep Marine Shale Formations: A Case Study of the Longmaxi Formation, Dingshan Area. *China Front. Earth Sci.* **2022**, *9*, 808535.
45. Sakhno, I.G.; Molodetskyi, A.V.; Sakhno, S.V. Identification of material parameters for numerical simulation of the behavior of rocks under true triaxial conditions. *Naukovyi Visnyk NHU* **2018**, *5*, 48–53. https://doi.org/10.29202/nvngu/2018-5/4.
46. Zhu, B.; Weifeng, K.; Jiami, X.; Yanjun, S. Numerical simulation research of construction method for shallow buried large section tunnel. *Open Civ. Eng. J.* **2016**, *10*, 578–597. https://doi.org/10.2174/1874149501610010578.
47. Hoek, E.; Carranza-Torres, C.; Corkum, B. Hoek-Brown failure criterion—2002 edition. In: Proceedings of the 5th North American Rock Mechanics Symposium and the 17th Tunnelling Association of Canada Conference, NARMS-TAC, Toronto, ON, Canada, 7–10 July 2002; pp. 267–271.
48. Hoek, E.; Diederichs, M. Empirical estimates of rock mass modulus. *Int. J. Rock Mech. Min. Sci.* **2006**, *43*, 203–215. https://doi.org/10.1016/j.ijrmms.2005.06.005.
49. Bieniawski, Z.T. *Engineering Rock Mass Classifications*; Wiley: New York, NY, USA, 1989.
50. Sakhno, I.; Sakhno, S. Numerical studies of floor heave control in deep mining roadways with soft rocks by the rock bolts reinforcement technology. *Adv. Civ. Eng.* **2023**, *2023*, 2756105. https://doi.org/10.1155/2023/2756105.
51. Li, J.; Huang, Y.; Zhai, W.; Li, Y.; Ouyang, S.; Gao, H.; Li, W.; Ma, K.; Wu, L. Experimental study on acoustic emission of confined compression of crushed gangue under different loading rates: Disposal of gangue solid waste. *Sustainability* **2020**, *12*, 3911. https://doi.org/10.3390/su12093911.
52. Zhou, H.; Zhang, C.; Li, Z.; Hu, D.; Hou, J. Analysis of mechanical behavior of soft rocks and stability control in deep tunnels. *J. Rock Mech. Geotech. Eng.* **2014**, *6*, 219–226. https://doi.org/10.1016/j.jrmge.2014.03.003.
53. Josh, M.; Esteban, L.; Delle Piane, C.; Sarout, J.; Dewhurst, D.N.; Clennell, M.B. Laboratory characterisation of shale properties. *J. Pet. Eng.* **2019**, *88–89*, 107–124. https://doi.org/10.1016/j.petrol.2012.01.023.

54. Almisned, O.A.; Alqahtani, N. Rock analysis to characterize Saudi soft sandstone rock. *J. Petrol. Explor. Prod. Technol.* **2021**, *11*, 2381–2387. https://doi.org/10.1007/s13202-021-01160-y.
55. Liu, Q.; Liang, B.; Sun, W.; Zhao, H. Experimental study on the difference of shale mechanical properties, *Adv. Civ. Eng.* **2021**, *2021*, 6677992. https://doi.org/10.1155/2021/6677992.